

# 1 Regional temperature change potentials for short lived 2 climate forcings based on radiative forcing from multiple 3 models

4 Borgar Aamaas<sup>1</sup>, Terje K. Berntsen<sup>1,2</sup>, Jan S. Fuglestad<sup>1</sup>, Keith P. Shine<sup>3</sup>, William J.  
5 Collins<sup>3</sup>

6 <sup>1</sup>CICERO Center for International Climate Research, PB 1129 Blindern, 0318 Oslo, Norway

7 <sup>2</sup>Department of Geosciences, University of Oslo, Norway

8 <sup>3</sup>Department of Meteorology, University of Reading, Reading RG6 6BB, United Kingdom

9 *Correspondence to:* Borgar Aamaas (borgar.aamaas@cicero.oslo.no)

10 **Abstract.** We calculate the absolute regional temperature change potential (ARTP) of various short lived climate  
11 forcings (SLCFs) based on detailed radiative forcing (RF) calculations from four different models. The temperature  
12 response has been estimated for four latitude bands (90-28° S, 28° S-28° N, 28-60° N, and 60-90° N). The regional  
13 pattern in climate response not only depends on the relationship between RF and surface temperature, but also on  
14 where and when emissions occurred and atmospheric transport, chemistry, interaction with clouds, and deposition.  
15 We present four emissions cases covering Europe, East Asia, the global shipping sector, and the entire globe. Our  
16 study is the first to estimate ARTP values for emissions during Northern Hemisphere summer (May-October) and  
17 winter season (November-April). The species studied are aerosols and aerosol precursors (black carbon (BC),  
18 organic carbon (OC), SO<sub>2</sub>, NH<sub>3</sub>), ozone precursors (NO<sub>x</sub>, CO, volatile organic compound (VOC)), and methane  
19 (CH<sub>4</sub>). For the response to BC in the Arctic, we take into account the vertical structure of the RF in the atmosphere,  
20 and an enhanced climate efficacy for BC deposition on snow. Of all SLCFs, BC is the most sensitive to where and  
21 when the emissions occur, as well as giving the largest difference in response between the latitude bands. The  
22 temperature response in the Arctic per unit BC emission is almost 4 times larger and more than 2 times larger than  
23 the global average for Northern Hemisphere winter emissions for Europe and East Asia, respectively. The  
24 latitudinal breakdown gives likely a better estimate of the global temperature response as it accounts for varying  
25 efficacies with latitude. An annual pulse of non-methane SLCFs emissions globally (representative of 2008) leads  
26 to a global cooling. Whereas, winter emissions in Europe and East Asia give a net warming in the Arctic due to  
27 significant warming from BC deposition on snow.

## 28 1 Introduction

29 Climate is influenced by a multitude of emissions with varying impacts (e.g., Myhre et al., 2013). Emissions of  
30 short lived climate forcings (SLCFs), such as black carbon (BC), organic carbon (OC), SO<sub>2</sub>, NH<sub>3</sub>, NO<sub>x</sub>, CO, and  
31 volatile organic compounds (VOCs), affect the composition of the atmosphere primarily on time scales of days to  
32 a few months. CH<sub>4</sub> is included in the definition often also included because its lifetime of around 10 years is shorter  
33 than or comparable to climate response timescales for stabilizing the climate (Aamaas et al., 2016). The temporal  
34 variation in the geographical pattern of SLCF emissions has changed over time, with emissions typically being  
35 high in the early phases of industrialization, and then gradually being reduced due to air quality concerns and

36 technological improvements. Nevertheless, emissions are still growing in many parts of the world, and there is a  
37 growing focus politically to develop mitigation strategy for the SLCFs to achieve both improved air quality and  
38 slowing global warming (Schmale et al., 2014;Shindell et al., 2012;Stohl et al., 2015).

39 Due to the short atmospheric lifetimes, emissions of SLCFs lead to a spatial pattern in radiative forcing (RF) that  
40 is more inhomogeneous than for emissions of long-lived greenhouse gases such as CO<sub>2</sub>. While we focus on RF  
41 from large emission regions, Bowman and Henze (2012);Henze et al. (2012) showed that radiative forcing  
42 efficiencies can vary by 1000 % for much smaller emission regions. It is well established that there is not a close  
43 relationship between the RF pattern and the surface temperature response pattern, due to modifications by heat  
44 transport in the atmosphere and ocean and the spatial variability in climate feedbacks (e.g., Boer and Yu, 2003).  
45 However, as shown by Shindell and Faluvegi (2009) and Shindell (2012), it is possible to establish relationships  
46 between the RF pattern caused by a certain constituent component and the response in broad latitude bands.  
47 Recently, Najafi et al. (2015), have shown from observational and model data that there is a distinct difference in  
48 the Arctic response to the overall forcing by ozone, aerosols and land-use, compared to other latitude bands.

49 Emission metrics are simple tools based on comprehensive model simulations that relate emissions to a certain  
50 response (physical climate change or economic damage), e.g. Fuglestedt et al. (2003);Tol et al. (2012). The most  
51 widely used emission metric, the Global Warming Potential (GWP), is given by the integrated RF (over a time  
52 horizon of H years) in response to a pulse emission. Shine et al. (2005) introduced the Global Temperature change  
53 Potential (GTP), using the surface temperature change (after a time horizon of H years) for the response. Emissions  
54 metrics have typically estimated a global effect due to global emissions (e.g., Aamaas et al., 2013). A first step  
55 going beyond global means was to quantify the global response based on regional emissions for SLCFs  
56 (Fuglestedt et al., 2010;Collins et al., 2013;Aamaas et al., 2016). By introducing the concept of regional  
57 temperature potentials (RTP), Shindell and Faluvegi (2010) extended the metric concept to include regional  
58 responses (in terms of surface temperature change in broad latitude bands) from regional RFsto regional emissions.

59 In addition to the regionality, the timing of the SLCFs emissions matter. This is potentially important since the  
60 photochemistry in the atmosphere, lifetime, atmospheric transport and forcing efficiency is likely to vary between  
61 the seasons. As some sources (e.g. domestic heating and agricultural waste burning) have a large seasonal cycle,  
62 using seasonal RTP metrics might have a significant impact on the evaluation of cost-effectiveness of mitigation  
63 measures.

64 Here we use detailed multimodel calculations of the relationship between emission location and the resulting  
65 specific RF (RF per Tg/yr emissions) for SLCFs (Bellouin et al., 2016) (Sect. 2.1) and the regional climate  
66 sensitivities (e.g., Shindell and Faluvegi, 2009) to estimate ARTPs for a range of aerosols, aerosol precursors, and  
67 ozone precursors (BC, OC, SO<sub>2</sub>, NH<sub>3</sub>, NO<sub>x</sub>, CO, and VOC), and CH<sub>4</sub> (Sect. 2.2). While some of ourThe findings  
68 mostly confirm the results by Collins et al. (2013),our analysis and extend the global temperature responses  
69 estimated by build on that work in several ways Aamaas et al. (2016) to responses on latitude bands. Our study is  
70 the first to calculate ARTPs for NH<sub>3</sub> emissions. The treatment of BC in the Arctic is more complex which has a  
71 high influence on the ARTPs for BC. Aspects of the aerosol effects on ozone precursors are also novel. For the  
72 first time, we distinguish between ARTPs for emissions taking place during Northern Hemisphere (NH) summer  
73 (May-October) and winter (November-April). ARTP metrics are calculated for regional emissions from Europe,

74 East Asia and the shipping sector, as well as global emissions (Sect. 3.1). The ARTP values are applied to calculate  
75 regional temperature responses of global emissions in Sect. 3.2. We also make a comparison of ARTPs with  
76 AGTPs (Sect. 3.3). Uncertainties are discussed in Sect. 3.4, and we conclude in Sect. 4.

## 77 2 Material and methods

### 78 2.1 Radiative forcing

79 The RFs that are the basis for the ARTP calculations of the SLCFs are calculated using 4 different chemistry  
80 climate models or chemical-transport models presented by Bellouin et al. (2016); see details about the models in  
81 Table 1. RFs are produced based on a control simulation and numerous perturbation simulations that consider a  
82 20% emission reduction in one type of species and one region in NH summer or winter. The ECLIPSE emission  
83 dataset applied here was created with the GAINS (Greenhouse gas-Air pollution Interactions and Synergies) model,  
84 see Stohl et al. (2015). The regional RFs are then averaged for pattern of the RFs is taken into consideration with  
85 four latitude bands, southern mid-high latitudes (90-28° S), the Tropics (28° S-28° N), northern mid-latitudes (28-  
86 60° N), and the Arctic (60-90° N), as forcing-response coefficients are only available for those latitude bands in  
87 the literature (e.g., Shindell and Faluvegi, 2010; Shindell, 2012).

88 We compute ARTPs for six different effectsprocesses that contribute to the RF for each species (aerosol effects,  
89 BC deposition on snow, BC semi-direct, short-lived ozone, methane, and methane-induced ozonesee Fig. 1 for  
90 details). The quantification of these effectsprocesses are given by the RF data from Bellouin et al. (2016). For the  
91 general circulation models, the RFs of the aerosol perturbations are calculated online using two calls to the  
92 radiation scheme. This method involves diagnosing radiative fluxes with and without the perturbation. These RFs  
93 do not include rapid adjustments (even in the stratosphere). For the OsloCTM2 chemistry transport model and the  
94 RF exerted by the ozone precursors in all the models, RF is computed by offline radiative transfer codes. The RF  
95 for methane is based on the analytical expression that includes stratospheric adjustments (Myhre et al., 1998),  
96 which gives a global mean. Based on this global RF estimate, we apply the latitudinal pattern in RF for methane  
97 and methane-induced ozone response in Collins et al. (2013). This pattern is based on an ensemble of 11 global  
98 chemical transport models that evaluated a global reduction of CH<sub>4</sub> mixing ratio, where RF was calculated using  
99 the method developed by the NOAA Geophysical Fluid Dynamics Laboratory (Fry et al., 2012).

100 For aerosols and aerosol precursors, all four models calculate the aerosol direct and 1<sup>st</sup> indirect (cloud-albedo)  
101 effect, except ECHAM6 which only includes direct RF. In this study, we group together the aerosol direct and 1<sup>st</sup>  
102 indirect (cloud-albedo) effect and name this process aerosol effects. In addition, OsloCTM2 estimated the RF from  
103 BC deposition on snow and the semi-direct effect. The semi-direct effect is quantified in Bellouin et al. (2016) by  
104 prescribing control and perturbed distributions of BC mass-mixing ratios based on OsloCTM2 in 30-year, fixed  
105 sea-surface simulations with the Community Earth System Model (CESM). The RF from aerosol-radiation  
106 interactions was quantified with multiple calls to the radiation scheme. Because the semi-direct effect is not  
107 included in the CAM4 component of the CESM, the semi-direct effect is calculated as the difference between the  
108 RF from aerosol-radiation interactions and the effective RF in the CAM4 model and using 30-year simulations  
109 with fixed sea surface temperatures to suppress the long-term response. For the ozone precursors and CH<sub>4</sub>, the  
110 total RF takes into account the aerosol direct and 1<sup>st</sup> indirect effects, short-lived ozone effect, methane effect, and  
111 methane-induced ozone effect. The ozone precursors and CH<sub>4</sub> can influence the aerosol effects, as a reduction in

112 [CH<sub>4</sub> concentration leads to increase in OH, which promotes sulfate aerosol formations](#). Only OsloCTM2 includes  
113 an estimate for nitrate aerosols, which is added to the *aerosol effect* quantification in the other models.

114 The best estimate of a species' RF has been calculated as the sum of all [effectprocesses](#), in which the average  
115 across the models is used for each [effectprocess](#). Not all models have estimated RFs for all species and  
116 [effectprocesses](#). In addition, ECHAM6 is excluded in the best estimate for BC, OC, and SO<sub>2</sub>, since it did not  
117 estimate the 1<sup>st</sup> indirect effect. For BC deposition on snow, the BC semi-direct effect, and nitrate aerosol, the best  
118 estimate is solely based on the OsloCTM2 model, while the best estimate are based on three models for all other  
119 [effectprocesses](#) (*aerosol effects*, short-lived ozone, methane, and methane-induced ozone).

120 For the high and low estimates of RF for each emission case, we find these values by taking the sum of the highest  
121 and lowest values, respectively, from all models for each individual [effectprocess](#).

122 The emission regions are defined according to tier1 Hemispheric Transport of Air Pollution (HTAP) regions (see  
123 Bellouin et al., 2016). Europe is defined as Western and Eastern Europe up to 66°N including Turkey. East Asia  
124 includes China, Korea, and Japan. Shipping is the global shipping sector. The global emissions category excludes  
125 this shipping activity. As RF values are also available for the remaining land areas outside of Europe and East  
126 Asia, results from the rest of the World are presented in SI Sect. 2.

## 127 **2.2 Regional temperature change potentials**

128 The regional temperature response has been calculated on the basis of RF in the latitude bands and regional climate  
129 sensitivities, as well as the temporal evolution of an idealized temperature response. Even though our estimates  
130 are based on seasonal emissions, the temperature responses calculated are annual means. The general expression  
131 for the ARTP following a pulse emission of [constituentcomponent](#)  $i$  ( $E_i$ ) in region  $r$  which leads to a response in  
132 latitude band  $m$  is (e.g., Collins et al., 2013):

$$133 \text{ARTP}_{i,r,m,s}(H) = \sum_l \int_0^H \frac{F_{l,i,r,s}(t)}{E_{i,r,s}} \times \text{RCS}_{i,l,m} \times R_T(H-t) dt \quad \text{_____} (1)$$

134  $F_{l,r,s}(t)$  is the RF in latitude band  $l$  due to emission in region  $r$  in season  $s$  as a function of time ( $t$ ) after the pulse  
135 emission  $E_{r,s}$  (in Tg). [Our study separates between four latitude response bands, in line with the typical width of](#)  
136 [response bands to inhomogeneous forcing found by Shindell et al. \(2010\), while more detailed modelling will be](#)  
137 [possible with a finer-masked RCS matrix available](#). The  $\text{RCS}_{i,l,m}$  is a matrix of regional response coefficients based  
138 on the RTP concept (unitless, cf. Collins et al., 2013). As these response coefficients are here normalized, they  
139 contain no information on climate sensitivity, only the relative regional responses [in the different latitude](#)  
140 [bandspattern](#). The global climate sensitivity is included in the impulse response function  $R_T$ , which is a temporal  
141 temperature response to an instantaneous unit pulse of RF (in K/(Wm<sup>-2</sup>)). We assume that the time evolution of  
142 temperature in each response band follows the global-mean time evolution. Cherubini et al. (2016) [show that this](#)  
143 [simplification is problematic for the first 5-10 years after emissions, but leads to less uncertainty after 20 years,](#)  
144 [which is our focus](#). We base our temperature response on that of the HadCM3 climate model (Boucher and Reddy,  
145 2008) with an equilibrium climate sensitivity of 1.06 K/(W m<sup>-2</sup>), which translates to a 3.9 K warming for a doubling  
146 of CO<sub>2</sub> concentration. This is the same climate sensitivity as for our absolute Global Temperature change Potential  
147 (AGTP) calculations on the same RF dataset (Aamaas et al., 2016).

148 Regional temperature responses at time  $t$  of an emission scenario  $E(t)$  can be calculated with these ARTP values  
 149 by a convolution (see also Aamaas et al., 2016). The temperature response is:

$$150 \Delta T_{i,r,m,s}(t) = \int_0^t E_{i,r,s}(t') \times ARTP_{i,r,m,s}(t - t') dt' \quad \text{_____} (2)$$

151 **2.2.1 For species with lifetimes less than one year**

152 For SLCFs with atmospheric lifetimes (or indirect effects causing RF) much shorter than both the time horizon of  
 153 the ARTP and the response time of the climate system (given by the time constants in  $R_T$  above), the general  
 154 expression for the ARTP can be simplified to (see Appendix 2 in Fuglestad et al., 2010):

$$155 ARTP_{i,r,m,s}(H) = \sum_l \frac{F_{l,i,r,s}}{E_{i,r,s}} \times RCS_{i,l,m} \times R_T(H) \quad (3)$$

156  $F_{l,i,r,s}$  is the RF over a year where emissions of constituent component  $i$  ( $E_{i,r,s}$  in Tg/yr) in emission region  $r$  occur  
 157 during season  $s$ , either during NH summer or winter.

158 **2.2.2 For species that affect methane**

159 Methane has an adjustment time comparable to the time horizon of the ARTP and the response time of the climate  
 160 system. So, for species that affect methane, an additional impulse response function that describes the atmospheric  
 161 decay of methane must be included ( $R_F$ ). In this case, we add such a function, which governs the methane and  
 162 methane-induced ozone effects for the ozone precursors (NO<sub>x</sub>, CO, and VOC) and CH<sub>4</sub>.

$$163 R_F(t) = e^{-t/\tau} \quad (4)$$

164 where  $\tau=9.7$  yr is the average adjustment time for methane in the three models (see Table 7 in Bellouin et al.,  
 165 2016). If we use the adjustment time of 12.4 yr from Myhre et al. (2013), the ARTP values would be larger. For  
 166 these species, this additional temperature perturbation due to these effects/processes has to be included:

$$167 ARTP(R_F \text{ response})_{i,r,m,s}(H) = \sum_l \int_0^H \frac{F_{l,i,r,s}}{E_{i,r,s}} \times R_F(H-t) \times RCS_{i,l,m} \times R_T(H-t) dt$$

$$168 \quad (5)$$

169 **2.2.3 Forcing-response coefficients**

170 The unitless regional sensitivity matrix ( $RCS_{i,l,m}$ ) is estimated based on literature values of regional response  
 171 coefficients in K/(W m<sup>-2</sup>) (see Sect. 1 in Supporting Information for tabulated coefficients). All these response  
 172 coefficients from the different literature sources have been normalized to the global response in those studies.  
 173 While the specific regional response coefficients have been estimated in other studies based on climate sensitivities,  
 174 the normalization to the global response removes the implicit climate sensitivities in the RCS values. We apply  
 175 several adjustments and refinements of the RCS values (see this section and Sect. 2.2.4); in each case, we normalize  
 176 the response coefficients and make sure that the climate sensitivity in our ARTP calculations is only included  
 177 in one of the parameters, in the temporal temperature response incorporated in ( $R_T$ ).

178 As such, RCS matrices only exist for annual emissions, we assume we can apply the same set of matrices for  
 179 emissions during NH summer and winter. This assumption is a simplification, but is done implicitly when the  
 180 annual mean RCS are applied to seasonal varying sources, e.g., wood burning heating stoves. We believe that  
 181 calculating explicitly the RF from each season improve the overall ARTP values. For the scattering aerosols and  
 182 aerosol precursors (SO<sub>2</sub>, OC, NH<sub>3</sub>), we use the coefficients tabulated in Shindell and Faluvegi (2010), which are

183 the mean responses of CO<sub>2</sub> and SO<sub>2</sub>. The same values are used for the longer-lived effects (methane and methane-  
 184 induced ozone) of the ozone precursors and CH<sub>4</sub>. For the short lived effects of the ozone precursors and CH<sub>4</sub>, we  
 185 apply the O<sub>3</sub> coefficients in Shindell and Faluvegi (2010) as tabulated in Collins et al. (2013).

186 For BC, the regional sensitivity matrix ~~applied is more complex is based on several sources~~, and the details for the  
 187 Arctic-to-Arctic responses are described in Sect. 2.2.4. For other latitude bands, the matrix for the BC aerosol  
 188 effects is given by BC forcing-response coefficients from Shindell and Faluvegi (2009) as tabulated in Table 3 in  
 189 Collins et al. (2013). ~~As we are not aware of a RCS matrix for RF explicitly calculated for the semi-direct effect,~~  
 190 ~~we use and the matrix for the semi-direct effect is from~~ the average CO<sub>2</sub> and SO<sub>2</sub> coefficients shown in Shindell  
 191 and Faluvegi (2010) based on Shindell and Faluvegi (2009). The semi-direct effect can potentially be included  
 192 either in the response based on RCS values or in the RF. Our approach is to include the semi-direct effect in the  
 193 RF and not in the RCS values, see next paragraph for details. The relationship for the deposition of BC on snow  
 194 is also given by the CO<sub>2</sub> coefficients shown in Shindell and Faluvegi (2010). For the snow albedo effect, we have  
 195 assumed an efficacy of 3 for all RF occurring outside of the Arctic (Myhre et al., 2013).

196 Our method differs from Shindell and Faluvegi (2009) as we have calculated the semi-direct effect independently.  
 197 Since Shindell and Faluvegi (2009) did not have any rapid adjustments in their sensitivities on RFs, the rapid  
 198 adjustments are implicitly included in their sensitivity coefficients. The reason is that in the GCM simulations used  
 199 to calculate the forcing-response coefficients (Shindell and Faluvegi, 2009; Flanner, 2013), semi-direct effects are  
 200 treated as feedbacks and as such they are included in the forcing-response coefficients. When we normalize to the  
 201 global response to find the RCS coefficients, we normalize on the global CO<sub>2</sub> response given by Shindell and  
 202 Faluvegi (2009) for all the species to avoid double counting.

#### 203 **2.2.4 Refinement of Arctic Response to BC**

204 We ~~apply~~ two refinements of the forcing-response coefficients for RFs occurring in the Arctic, one for the  
 205 *aerosol effects* in the atmosphere and one for the effects due to BC on snow. We first discuss how we handle the  
 206 *aerosol effects* in the atmosphere.

207 For BC in the Arctic, the forcing by absorption takes place in a generally stably stratified atmosphere (Quinn et al., 2008).  
 208 The transport of BC to the Arctic occurs approximately along isentropic surfaces; thus emissions from  
 209 East Asia are generally at a higher altitude than emissions from Europe. The BC particles cause also dimming at  
 210 the surface. In the Arctic, heat is not easily mixed down to the surface. The efficacy of BC forcing depends highly  
 211 on the altitude of the BC (Flanner, 2013; Lund et al., 2014; Sand et al., 2013). To account for this the RTP concept  
 212 is modified for BC forcing in the Arctic. The contribution by RF exerted in the three latitude bands outside the  
 213 Arctic-to-Arctic warming ( $ARTP(ex-Arc)_{BC,r,Arc,s}$ ) is calculated with the standard method using RTP-coefficients  
 214 from Shindell and Faluvegi (2010), as described in Sect. 2.2.3:

$$215 \quad ARTP(ex - Arc)_{BC,r,Arc,s}(H) = \sum_{l=1}^3 \frac{F_{l,BC,r,s}}{E_{BC,r,s}} \times RCS_{BC,l,Arc} \times R_T(H) \quad (6)$$

216 For the RF within the Arctic the response ( $ARTP(Arc)_{BC,r,Arc,s}$ ) is calculated according to Eq. (7) following the  
 217 method presented in Lund et al. (2014):

$$218 \quad ARTP(Arc)_{BC,r,Arc,s}(H) = \sum_z \frac{F^{(z)}_{Arc,BC,r,s}}{E_{BC,r,s}} \times RCS(z)_{BC,Arc,Arc} \times R_T(H) \quad (7)$$



219 Both the RF ( $F(z)_{Arc,BC,r,s}$ ) and the regional sensitivity matrix ( $RCS(z)_{BC,Arc,Arc}$ ) have a dependence on the height of  
220 the BC which is denoted by the  $z$  in Eq. (7). We apply a vertically-resolved regional sensitivity matrix based on  
221 Fig. 2(a) in Lund et al. (2014), which shows the sensitivity of the Arctic surface temperature response to the altitude  
222 of RF in the Arctic from Flanner (2013) interpolated to the vertical structure in OsloCTM2. This relationship can  
223 be combined with the normalized BC RF from Samset and Myhre (2011) to give a normalized Arctic surface  
224 temperature response to BC perturbations at different altitudes.

225 We apply the vertical profile of BC concentration in the Arctic for all three models used. These vertical profiles  
226 are converted into RF profiles based on the vertically resolved RF to burden ratio in OsloCTM2.

227 Our second refinement is on the forcing-response coefficients for BC on snow in the Arctic, where we use the  
228 forcing-response sensitivity found by Flanner (2013).

229 As the semi-direct effect is implicitly included in the estimates [for the BC aerosol effects for Arctic-to-Arctic](#)  
230 [warming](#) from Flanner (2013), we cannot distinguish between direct RF and semi-direct RF for RF occurring in  
231 the Arctic. The Arctic RF due to the semi-direct effect provided in Bellouin et al. (2016) is left out to avoid double  
232 counting. However, our argument is that the explicit vertically resolved forcing-response relationships is a much  
233 better fit than a vertically averaged forcing-response relationships, which makes this the preferable method. As a  
234 result, this study's ARTP estimates of the semi-direct effect in the Arctic is due to the semi-direct RF from outside  
235 the Arctic.

236 The Flanner (2013) study is based on an equilibrium climate sensitivity of  $0.91 \text{ K}/(\text{W m}^{-2})$ , which is 14% lower  
237 than applied in our study. We adjust our calculations so that the climate sensitivity is in line with the rest of our  
238 calculations (Boucher and Reddy, 2008). The correction is done with a two-layer box-diffusion model based on  
239 the parameters of the Hadley Centre model (see Aamaas et al., 2013), which also modifies the timescales of the  
240 impulse response function.

241 The total response in the Arctic is then the sum of the contributions from BC forcing outside of the Arctic and  
242 inside of the Arctic.

$$243 \quad ARTP_{BC,r,Arc,s}(H) = ARTP(ex - Arc)_{BC,r,Arc,s}(H) + ARTP(Arc)_{BC,r,Arc,s}(H) \quad (8)$$

## 244 **3 Results**

### 245 **3.1 ARTP values**

#### 246 **3.1.1 Best estimates**

##### 247 **Results for ARTP(20)**

248 The best estimates of ARTP values for a time horizon of 20 years are presented in Fig. 1, for each of the four  
249 emission regions, the four response bands, plus the global mean, for all emitted species considered here. We  
250 provide values for other time horizons (10, 50 and 100 years) in Supporting Information Sect. 2. The rationale for  
251 highlighting 20 years is that if the focus is to be placed on mitigation of SLCFs then it is more appropriate to  
252 investigate climate impacts on short timescales. [Results for cE](#) continuous time horizons between 1-50 years are  
253 given in Sect. 3.1.5.

254 The uncertainties in Fig. 1 are given as a range following the differences in RFs estimated between the models.  
255 We acknowledge other uncertainties, such as for climate sensitivity, which are discussed in Sect. 3.4. The  
256 uncertainty is often larger than the variation between different emission regions, seasons, and responses in the  
257 latitude bands. However, we will show in Sect. 3.1.4 that the relative variations between the best estimates for  
258 individual species are often robust. As ARTP values for the shipping sector are based on only two RF estimates,  
259 uncertainty ranges are not given for shipping. The robustness in the best estimate for shipping is likewise lower  
260 than for ~~the other~~ differences ~~regions~~. E.g., these two models disagree for shipping on the sign for the *aerosol effect*  
261 of NO<sub>x</sub> emissions. NH<sub>3</sub> estimates are also from one model only, and are not shown for shipping (because emissions  
262 from that sector are negligible).

### 263 **Response patterns**

264 For emissions from a given region, the latitudinal response pattern is partly governed by the pattern of RF and  
265 partly the pattern in the forcing-response coefficients. The RF signal is mainly located in the latitude bands near  
266 the emission sources for the short-lived constituent~~components~~, while it is more evenly distributed for  
267 effects~~processes~~ linked to methane. Hence, as shown in Bellouin et al. (2016) (see especially their Fig. 7),  
268 emissions in Europe and East Asia give largest RF in the NH mid-latitude band and the smallest in the Southern  
269 Hemisphere (SH) mid-high latitudes. Due mainly to heat transport between the latitude bands, the RCS coefficients  
270 also represent non-local temperature responses, thus, the temperature response is seen more evenly in all latitude  
271 bands~~Due to heat transport between the latitude bands and the temperature response lasting over several years, the~~  
272 ~~forcing response is averaged out over several latitude bands by the temperature response~~. Nevertheless, the  
273 temperature response has higher sensitivity towards the Arctic and NH mid-latitude bands (see all panels in Fig.  
274 1) as a result of local feedback processes being stronger in the Arctic, driven by local cloud, water vapor, and  
275 surface albedo feedbacks (Boer and Yu, 2003).

276 We next consider differences between the emission regions Europe and East Asia. The RF per unit emission is  
277 dependent on where the emissions occur, which causes differences in the ARTP(20) values. The differences in the  
278 global average of RFs and global emission metric values such as AGTP(20) are discussed in Aamaas et al. (2016).  
279 In short, the emission metric values for the aerosols are larger for European than East Asian emissions, but not for  
280 NH<sub>3</sub> in winter. Variations are also seen for the ozone precursors, but these differences are relatively smaller  
281 between European than East Asian emissions for CO and VOC than for the aerosols. For CO, East Asia has  
282 marginally larger values (see Figs. 1(K) and 1(L)) and marginally larger for European VOC emissions (see Figs.  
283 1(M) and 1(N)). The main difference in the global average of ARTP values calculated here and the AGTP values  
284 calculated in Aamaas et al. (2016) is the much larger impact for BC deposition on snow for ARTP (see Fig. 1(B)),  
285 as the AGTP study did not account for the increased efficacy of BC deposition on snow.

286 The timing of emissions also influences the RF per unit emissions. The emission metric values for the aerosol  
287 emissions in Europe and East Asia (see Figs. 1(A)-1(F)) are larger for summer than winter, except for BC. For the  
288 aerosols, the aerosol RF is driven by seasonal variations in the incoming solar radiation. More sunlight in local  
289 summer results in stronger RFs (Bellouin et al., 2016). Seasonal differences in atmospheric lifetimes due to  
290 seasonality in precipitation may also contribute. BC is discussed in detail in Sect. 3.1.2.



291 For the ozone precursors (see Figs. 1(I)-1(N)), the largest values occur in winter for CO (Figure 1(L)) and in  
292 summer for VOC (Figure 1(M)). CO has a longer lifetime during local winter leading to a larger fraction of the  
293 CO emitted being transported from the higher latitudes to the Tropics. Here, the effects of CO-oxidation on tropical  
294 OH have the largest impacts on the methane lifetime.

295 The latitudinal response patterns are similar for the different species. For all the species, the response bands with  
296 the largest ARTP values are for the responses in the NH mid-latitudes (60% of the cases) and Arctic and the band  
297 with the least response the SH mid-high latitudes (see all panels in Fig. 1). This skewness towards the NH is partly  
298 due to the emissions occurring in the NH for Europe and East Asia, as well as mainly for the global emissions in  
299 the NH, but the same pattern is seen for CH<sub>4</sub> (Figure 1(O)), for which the emission location is less important.  
300 Further, the high ARTP values for the Arctic are also due to stronger local feedback processes, leading to larger  
301 forcing-response sensitivities, while high ARTP values for the NH mid-latitudes are a combination of high RF  
302 values per unit emission and relatively large regional climate sensitivities. Shindell et al. (2015) argue that the high  
303 responses in NH mid- and high-latitudes are not due to feedbacks particular for the SLCFs, but mainly due to the  
304 efficacies driven by the large land fraction in this area and strong snow albedo feedbacks. The low ARTP values  
305 for SH mid-high latitudes is caused by a combination of most emissions occurring in NH for the emission regions  
306 and weaker forcing-response coefficients in SH. Let us consider OC emissions in East Asia during summer as an  
307 example with RF mostly in one band. The RF (see Bellouin et al., 2016) in the NH mid-latitude band is 260%  
308 above the global average, practically zero in the SH mid-high latitude band and about 50% below the global  
309 average in the other two bands. This skewedness is also modeled in the ARTP (see Fig. 1(C)), but with more  
310 emphasis on the Arctic. The ARTP value for the responses in the Arctic and NH mid-latitudes is about 70% and  
311 90% above the global average, respectively. In the SH mid-high latitudes response band, the ARTP value is about  
312 20% of the global average. At the other end of the range, emissions of CH<sub>4</sub> have a global impact due to the  
313 atmospheric lifetime of CH<sub>4</sub> (9.7 years). The RF in the Arctic band is 35% below the global average, while 25%  
314 above in the Tropics. But the weighing is almost opposite for the ARTP, as the Arctic response band has a ARTP  
315 value 34% above the global average and the Tropics 13% above the average (see Fig. 1(O)). For the SH mid-high  
316 latitude response band, both the RF and ARTP are lower than the global average, by -35% and -49%, respectively.

317 For most of the aerosol emissions (see Figs. 1(A)-1(F)), the ARTP values for the *aerosol effects* component are  
318 larger for emissions in NH summer than winter, even in the Tropics for emission from both Europe and East Asia.  
319 The only exception is NH<sub>3</sub> (Figures 1(G) and 1(H)), which has a larger ARTP value for winter than summer for  
320 East Asian and global emissions. Longer sunlight duration in the summer hemisphere yields stronger RFs (Bellouin  
321 et al., 2016), which impact the ARTP value for the response even in the Tropics. This general observation does  
322 not hold for BC when we include the effectprocess “BC deposition on snow”, as this effectprocess is largest in NH  
323 winter when the snow cover area is at its largest.

324 The ARTP(20) values shift sign for some of the latitude response bands. VOC emissions generally lead to a  
325 warming, however, our best estimate indicates a small cooling in SH mid-high latitudes for European and East  
326 Asian winter emissions (Figure 1(N)). The negative RF for the *aerosol effect* in this response band is driving this  
327 cooling as the other perturbations have a small impact on the response in the SH mid-high latitudes. VOC emissions  
328 perturb aerosols via secondary organic aerosol formation, which two out of three models find to be cooling. For

329 the ozone precursors, the *aerosol effects*, and the short-lived ozone effect to a smaller degree, also shift between  
330 warming and cooling depending on the latitude response band.

### 331 **3.1.2 Variation of BC response with emission season and region**

332 The largest differences in ARTP(20) values are seen for BC, such as the timing of emissions (comparing Figs. 1(A)  
333 and 1(B)) ~~and~~, the location during winter (comparing the different emission regions in Fig. 1(B)), and response  
334 regions (comparing Arctic with other latitude bands for European emissions in Fig. 1(B)).

335 The total emission metric values of BC emissions depend on which effectsprocesses are included. The direct  
336 *aerosol effect* is larger for summer than winter emissions. The direct temperature response is similar for emissions  
337 occurring in Europe, East Asia, and globally. Similarly, the semi-direct effect is most pronounced in summer as  
338 this effect is driven by absorption of shortwave radiation. When the influence from the BC deposition on snow is  
339 included, the ARTP value increases significantly for emissions during NH winter. For emissions in Europe, the  
340 global temperature response to the semi-direct effect is -46% and -12% of the *aerosol effect* in summer and winter,  
341 respectively, and the deposition on snow effect 12% and 230% of the *aerosol effect* in summer and winter,  
342 respectively. The relative share of the deposition on snow effect is 60 % lower for winter East Asian emissions  
343 than for winter European emissions. The semi-direct effect has a relative weight of -56% compared to the *aerosol*  
344 *effect* for the global ARTP(20) East Asian emissions in summer and close to zero in winter. The impact of BC  
345 deposition on snow is largest when large snow and ice covered surface areas and solar radiation at the BC  
346 deposition location is combined, such as in late winter. The response from European emissions is larger than for  
347 East Asian emissions since the emission region is closer to the Arctic, which makes BC transport into the sensitive  
348 Arctic more likely (Sand et al., 2013). The effect of the BC deposition on snow dominates the winter-summer  
349 difference for BC and hence our results are sensitive to both the calculated RF and efficacy for this BC process.

350 The Arctic response amplification, i.e., how much stronger the response is in the Arctic relative to the global  
351 average, is largest for winter emissions as the deposition on snow effect is relatively larger than for summer  
352 emissions. The total Arctic response amplification for BC is for European emissions 240% and 390% larger than  
353 the global average in summer and winter, respectively, and for East Asian emissions 160% and 240% larger than  
354 the global average in summer and winter, respectively. As a result, wintertime BC emissions have the largest  
355 latitudinal variation in the ARTP(20) amongfor all SLCFs. This Arctic amplification is driven by the temperature  
356 response from deposition on snow effect (almost 500% for European emissions and 400% for East Asian emissions  
357 for this effectproecess), which is largest in the Arctic response band, above the global average in the NH mid-  
358 latitude, and below average in the two other response bands. Latitudinal response variations are also found for the  
359 other effectsprocesses, but relatively much smaller.

### 360 **3.1.3 Comparison with Collins et al. (2013)**

361 Our findings are largely consistent with those by Collins et al. (2013). Similarities occur because the two studies  
362 share some of the same forcing-response coefficients\_(Shindell and Faluvegi, 2009) and climate sensitivity  
363 (Boucher and Reddy, 2008). In this work, we have more detailed estimates for a more detailed treatment of BC in  
364 the Arctic and we include NH<sub>3</sub>, as well as more detailed for aerosol impacts on ozone precursors. ARTP values  
365 are also given for two seasons, for the shipping sector and our global estimate include all emissions. The study by  
366 Collins et al. (2013) is more comprehensive than our study in terms of the number of models included, while the

367 RF dataset we use is newer and more detailed (see Table 1 in Bellouin et al., 2016) and the forcing-response  
368 coefficients are improved. Hence, results from both studies will be of benefit to those wanting to apply our metrics.

369 The ARTP(20) values in Collins et al. (2013) are mostly lower than the average response of annual emissions in  
370 this study, while the variations between the latitude response bands are mostly similar. We model 180% and 80%  
371 stronger global temperature sensitivity from European and East Asian emissions of BC. The largest difference is  
372 that our study included the response from BC deposition in snow whereas Collins et al. (2013) did not. In addition,  
373 Collins et al. (2013) applied a forcing-response coefficient for the BC direct RF that gives an Arctic cooling due  
374 to emissions in the Arctic (Shindell and Faluvegi, 2009). When including a more detailed parameterization for  
375 atmospheric BC in the Arctic that considers the height of the BC (see Sect. 2.2.4), the global temperature response  
376 of BC emissions increases by 4-14%. The difference is much larger in the Arctic, and the increase in the Arctic is  
377 22-210% when only considering the BC direct and 1<sup>st</sup> indirect effects.

#### 378 **3.1.4 Robustness for individual species**

379 The differences between ARTP(20) values for different emission regions and emission seasons, as well as for the  
380 response in different latitude bands for one set of emissions, are smaller than the inter-model uncertainty ranges.  
381 However, the ARTPs based on RFs for the individual models agree often with the best estimate on the ranking  
382 between the different emission and response cases, which strengthens our confidence that the variations calculated  
383 for the best estimate are robust. In Supporting Information Sect. 3, we quantify this robustness and find a high  
384 robustness consistent with similar analysis done on AGTP(20) values (Aamaas et al., 2016). As the temperature  
385 response is more smeared out globally for the ozone precursors than for the aerosols, the models agree to a larger  
386 extent for the aerosols concerning which latitude response bands see the largest and smallest temperature  
387 perturbations. For BC, we compare results only including the *aerosol effects* as only one model includes BC on  
388 snow and semi-direct effects. The model NorESM has the largest discrepancy relative to the best estimate for NO<sub>x</sub>  
389 and VOC, while HadGEM3 disagrees the most for CO.

#### 390 **3.1.5 Variations with time horizon**

391 We have so far only analyzed ARTP(20) values. Here we present results for a range of time horizons up to 50  
392 years in Fig. 2. The ARTP values vary greatly with time horizon and generally decrease in magnitude with time  
393 for SLCFs, especially for the aerosols (see Figs. 2(A) and 2(B) for BC). The ranking between different regions,  
394 seasons and latitude bands also changes with varying time horizon for the ozone precursors (see Figs. 2(C)-2(H)).  
395 The reason is that the aerosols and aerosol precursors have atmospheric lifetimes of about a week, while methane  
396 has an atmospheric perturbation lifetime of almost 10 years, which will lead to variations in the relative weight of  
397 the short-term and long-term effects ~~processes~~ with varying time horizons for the ozone precursors (e.g., Collins et  
398 al., 2013).

399 The result ~~temporal variability~~ shows that NO<sub>x</sub> emissions in Europe have in general more ~~the most~~ negative ARTP  
400 values for summer emissions than for winter emissions ~~for all time horizons~~, which is due to a stronger methane  
401 effect (Figure 2(C)). For East Asian emissions, the situation is mixed with the most negative ARTP values in the  
402 first 10-15 years for winter emissions, while summer emissions have the most negative values for longer time  
403 horizons (Figure 2(D)). For summer emissions, ARTP values in the first few years is pushed upwards by stronger  
404 solar insolation than in winter leading to more short-lived ozone. For the ozone precursors, the ranking on which  
405 latitude band is the most sensitive is mostly unchanged after 5 years, but can vary in the first years.

### 406 3.2 Regional temperature response for 2008 emissions

407 Given the ARTP values, we calculate the regional and global temperature responses due to real-world emissions  
408 of SLCFs based on Eq. (2). The temperature response at time  $H$  in latitude band  $m$  for an emission  $E$  of species  $i$   
409 is

$$410 \Delta T_{i,r,m,s}(H) = E_{i,r,s} \times ARTP_{i,r,m,s}(H) \quad (9)$$

411 We estimate the temperature response in the four latitude bands for a time horizon of 20 years given real-world  
412 pulse emissions in 2008 from Europe, East Asia, the shipping sector, and globally (Klimont et al., In prep.). The  
413 global emissions are given in Supporting Information Table S7. Such a view on regional responses is useful as  
414 regional variations will be hidden in the global mean response (e.g., Lund et al., 2012). The emissions include  
415 seasonal variability with emissions often being largest in the NH winter season. The temperature perturbations are  
416 mainly governed by the ARTP(20) values given in Sect. 3.1.1, but also by the seasonal cycle of the emissions. The  
417 emissions in Europe and East Asia are larger in winter than summer for all species except  $\text{NH}_3$ , driven by larger  
418 residential heating and cooking emissions during winter conditions. BC emissions are about 70% larger in winter  
419 than in summer, OC emissions 70-100% larger, and  $\text{SO}_2$  emissions almost 20% larger in East Asia and more than  
420 40% larger in Europe (Klimont et al., In prep.). The seasonal variability is smaller for all the ozone precursors, CO  
421 with the largest range (43% more in winter).

422 For the global source region, ignoring the seasonality by applying annually averaged emissions and ARTP values  
423 gives similar total temperature responses as treating the seasons separately and then averaging (differences of 0-  
424 3%). However, when treating Europe or East Asia individually seasonal information changes the temperature  
425 estimates by up to 18%. The difference is largest for the aerosols. For Europe, the temperature response increases  
426 by 8% for BC and decreases the cooling by OC by 10%. The largest relative changes are seen in the net temperature  
427 perturbation of all SLCFs.

428 Figure 3 shows that the temperature perturbations are smallest for the SH mid-high response latitudes and largest  
429 for the Arctic and NH mid-latitudes, as seen for ARTP(20). For most latitude response bands,  $\text{SO}_2$  has the largest  
430 impact, so the net effect of the seven SLCFs is a cooling in most of the cases. BC has the second largest impact  
431 with a warming that is largest for winter emissions. The shipping sector is dominated by cooling from  $\text{SO}_2$  and  
432  $\text{NO}_x$  (see Figs. 3(E) and 3(F)), while the other sectors have a much broader mix of species causing both heating  
433 and cooling. However,  $\text{NO}_x$  can be both warming and cooling depending on emission metric choices. For ARTP(20)  
434 applying sustained emissions,  $\text{NO}_x$  has a relatively smaller cooling impact and even contributes to warming in  
435 some latitude bands for shipping emissions in summer (see Supporting Information Fig. S1).

436 Emission of non- $\text{CH}_4$  SLCFs leads normally to net cooling or effects that cancel each other out. However, we  
437 show that some specific cases cause warming in the Arctic (see Figs. 3(B), 3(D), and 3(H)). Winter emissions in  
438 Europe and East Asia cause a warming in the Arctic and almost no net perturbation in the NH mid-latitudes and  
439 other bands. The main reasons for the seasonality differences are the strong heating from the BC deposition on  
440 snow for winter emissions close to snow and ice surfaces, as well as the relatively larger BC emissions in winter  
441 than for the other species, and weaker cooling effects of  $\text{SO}_2$  in winter. For summer emissions in Europe and East  
442 Asia (Figures 3(A) and 3(C)), the situation is the opposite with the largest cooling in the Arctic and NH mid-  
443 latitudes. A small net heating in the Arctic is also observed for global emissions in the NH winter season.

### 444 3.3 Global temperature response and comparing ARTP and AGTP

445 We discuss how adding complexity with four latitudinal response bands impacts the metric value by comparing  
446 the global temperature response for regional and seasonal emissions presented in Sect. 3.2 based on ARTP with  
447 the AGTP calculation in Aamaas et al. (2016). Shindell (2014) concluded that the efficacy of the temperature  
448 response depends on the location of the RF. As a result, more RF in the NH middle to high latitudes for the aerosols  
449 give a larger response than a globally averaged RF. Lund et al. (2012) found that an emission metric first based on  
450 regional variations, then averaged globally gives a more complete and informative value than one based on global  
451 mean inputs. Work by Stohl et al. (2015) shows that regional temperature estimates based on ARTPs mostly agree  
452 with calculations with earth system models. Although heterogeneity can be better included in temperature  
453 responses given by ARTPs compared to AGTPs, the superiority of ARTPs relative to AGTPs has not been tested  
454 thoroughly and confirmed. However, we argue that the global temperature response can be better quantified with  
455 ARTPs than AGTPs since a simple representation of varying efficacies due to heterogeneous RF is included.

456 How the global temperature responses are calculated given the AGTP values is shown in Supporting Information  
457 Sect. 6 and Aamaas et al. (2016). For the ARTP values, the global temperature is calculated from the area-weighted  
458 mean of the responses in the latitude bands. As the ARTP calculations are based on an efficacy of 3 for BC  
459 deposition on snow, the same efficacy is applied in the AGTP calculations. Our comparison between the methods  
460 applying ARTP and AGTP uses a pulse emission  $E$ . The difference in the global temperature perturbation ( $\Delta T(diff)$ )  
461 for species  $i$  between the two methods is then

$$462 \Delta T(diff)_{i,r,s}(H) = \sum_m E_{i,r,m,s} \times ARTP_{i,r,m,s}(H) - E_{i,r,s} \times AGTP_{i,r,s}(H), \quad (10)$$

463 which is applied for each emission region  $r$  and emission season  $s$ .

464 We compare the temperature perturbation based on ARTP and AGTP for a time horizon of 20 years using the 2008  
465 emissions. The largest difference is for NH summer emissions. For global NH summer emissions, ARTP(20) result  
466 in 17% more net cooling than AGTP(20) and about 26% and 32% more cooling for European and East Asian  
467 emissions, respectively. The differences in responses are smaller for NH winter emissions. Annually, global  
468 emissions lead to a 13% larger cooling based on ARTP than on AGTP. See Sect. 7 in Supporting Information for  
469 further details. The differences emerge because the patterns of RF and efficacy are correlated, with highest RFs  
470 and highest efficacies in the northern mid latitudes and Arctic. Thus, the ARTPs are necessary even to obtain a  
471 global temperature response since they account for these correlations.

472 Next, we analyze the differences between applying ARTP and AGTP for the individual species (see Fig. 4 and Fig.  
473 S3 in Supporting Information). The relative differences are in most cases similar for the different emission regions  
474 and seasons [for the same species](#), which show that the differences between ARTP and AGTP are governed by  
475 differences in the forcing-response coefficients between the two. The relative differences are generally larger for  
476 the aerosols than the ozone precursors, as seen in Fig. 4, where only the emissions regions and seasons with a  
477 relative difference larger than 20% are presented. The temperature responses are generally stronger for the  
478 scattering aerosols and the BC deposition on snow given the ARTP than the AGTPs, which is in line with greater  
479 efficacies due to rapid and strong feedbacks for RFs in the northern mid-latitudes and the Arctic latitude bands  
480 (Shindell, 2014). BC and ozone precursors are in general given lower weight when using ARTPs than AGTPs.  
481 Application of ARTP and AGTP values give variation of up to 30% for individual [effects/processes](#), with an

482 average of 12% for individual species. ARTPs are more detailed in nature and through accounting for variations  
483 in efficacy will give more realistic global temperature responses.

### 484 3.4 Uncertainties

485 The ARTP values calculated have uncertainties and limitations given by the uncertainties in each parameter on the  
486 right hand side of Eq. (1). The uncertainty ranges shown in Fig. 1 are based on the range in  $\frac{F_{Li}(t)}{E_i}$  across all  
487 contributing models. Bellouin et al. (2016) point out four important aspects regarding model diversity. Lifetime  
488 diversity is large, the unperturbed baseline causes diversity for non-linear mechanisms, the number of species  
489 included varies among the models, and finally the strength of the interactions between aerosols and chemistry  
490 differs among the models. The climate sensitivity included in  $R$  is 3.9 K for a doubling of CO<sub>2</sub> concentration  
491 (Boucher and Reddy, 2008); however, IPCC (2013) estimate the climate sensitivity to likely be in the range 1.5-  
492 4.5K. Uncertainty is also found in the time evolution of  $R_T$ . We have based this impulse response function on only  
493 one model, while Olivié and Peters (2013) have shown that this will vary between models. For instance, they found  
494 a spread in the GTP(20) value of black carbon of about -60 to +80% due to variability for  $R_T$  between models.  
495 However, the uncertainty in  $R_T$  is less relevant for the regional patterns. The forcing-response coefficients are also  
496 based mainly on one model (Shindell and Faluvegi, 2010). While we separate between emissions occurring during  
497 NH summer and winter season, forcing-response coefficients do not exist on a seasonal basis. Hence, the seasonal  
498 differences presented here in the ARTP values are not due to potential differences in the response sensitivities, but  
499 due to differences in the RF. Aamaas et al. (2016) observed that estimates of  $\frac{F_{Li}(t)}{E_i}$  tend to be correlated for different  
500 species in a model, which increases the uncertainty when a mitigation package is considered.

501 The temperature response will vary by species and location, such as land surface versus ocean surface. These  
502 differences are not accounted for in our study, but the increased efficacy in the RCS matrix towards the NH can  
503 be partly attributed to larger land area fraction in the NH (Shindell et al., 2015). The temperature increase is in  
504 general larger over land than ocean (Boer, 2011) driven by several local feedbacks (Joshi et al., 2008). We do not  
505 have data to break down this effect for our emission regions, but results in Shindell (2012) indicate that the land  
506 response may be 20 % larger than the average.

507 More research is warranted to improve the temperature estimates and to reduce uncertainties. As the forcing-  
508 response coefficients (RCS) come mainly from one model, research is most needed to test the robustness of those  
509 model results, preferably in a multimodel intercomparison framework. We would also like to encourage work on  
510 how the temporal temperature response varies between the different latitude bands and species. As new data on  
511 RF from more and smaller emission regions are published in the future, and if RCS values become available for  
512 additional forcing and response regions, our study could be extended with this improved data.

513 The ARTP values are given for large emission regions, while large variations are likely within the regions. The  
514 impact of emissions from an European city may be very different to the average we have estimated for European  
515 emissions (see Bowman and Henze, 2012; Henze et al., 2012). They found that the key determinants for aerosols  
516 are the aerosol lifetime, surface albedo, and the chemical environment. Latitude is a key variable for ozone, but  
517 atmospheric chemistry, altitude, and vertical mixing play also a role.



518 Ideally, calculations of the temperature response of changed emissions of SLCFs should use earth system models  
519 for the most correct estimates. However, this is extremely time consuming, and many emission perturbations will  
520 have small signal/noise ratios. Users of emission metrics, such as policymakers and decision makers, might not  
521 have the needed expertise to utilize advanced models. Although the ARTP calculations are simplifications and  
522 contain uncertainties, these emission metrics are useful, simple, and quick approximations for calculating the  
523 temperature response in the different latitude bands for emissions of single species or a mix of SLCFs (and long  
524 lived greenhouse gases).

#### 525 **4 Conclusion**

526 We have presented ARTP values in four latitude bands (90-28° S, 28° S-28° N, 28-60° N, and 60-90° N) for  
527 several SLCFs (BC, OC, SO<sub>2</sub>, NH<sub>3</sub>, NO<sub>x</sub>, CO, VOC, and CH<sub>4</sub>) based on four different models. Numbers are  
528 provided for emission occurring in Europe, East Asia, from the global shipping sector, as well as globally.  
529 Emissions were separated between the NH summer and winter seasons. Although ARTPs are simplifications, they  
530 are useful for analyzing the temperature response to possible mitigation strategies. The ARTP values are largest  
531 in the response bands Arctic and NH mid-latitudes and the smallest in the SH mid-high latitudes. The different  
532 models agree in most of the cases on the ranking of the temperature perturbation in the different latitude bands.

533 BC is the species that is the most sensitive to the timing of emissions, to the location during winter, as well as  
534 having the largest spread in responses between the latitude response bands in winter. The relative difference  
535 between the response bands is largest for BC emissions during NH winter, and ~~the more~~ the closer to the Arctic  
536 the emissions occur. The Arctic temperature response is 390% and 240% larger than the global temperature  
537 response for winter emissions in Europe and East Asia, respectively. BC deposition on snow is the most important  
538 ~~effectprocess~~ influencing the Arctic for BC emissions occurring in NH winter, both in absolute and relative terms.

539 We have also investigated how the global response based on ARTP compares with AGTP. Our study indicates  
540 that the global temperature response can be better quantified with ARTPs than AGTPs since ARTPs include a  
541 simple representation of varying efficacies due to heterogeneous RFs. For global emissions of SLCFs excluding  
542 CH<sub>4</sub>, calculations based on ARTP values give 13% larger cooling than based on AGTP values. Globally, both  
543 these calculations based on ARTP(20) and AGTP(20) show a cooling, while European and East Asian winter  
544 emissions give a small net warming or near zero impact according to ARTP. This is driven by net warming in the  
545 Arctic and close to zero perturbation in the other latitude bands. For summer emissions, net cooling occurs in all  
546 latitude bands, but are largest in the NH mid-latitudes and Arctic. Seasonal emissions and seasonal ARTP values  
547 give almost the same total temperature response as annual emissions and annual ARTP values for global emissions,  
548 but changes the temperature responses by up to 18% when looking at emissions from individual regions such as  
549 Europe and East Asia.

#### 550 **Acknowledgements**

551 The authors would like to acknowledge the support from the European Union Seventh Framework Programme  
552 (FP7/2007-2013) under grant agreement no 282688 – ECLIPSE, as well as funding by the Norwegian Research  
553 Council within the project “the Role of Short-Lived Climate Forcers in the Global Climate Regime” (project no.  
554 235548). We thank Nicolas Bellouin for providing RF data for all the models. In addition, we show our  
555 appreciation to Nicolas Bellouin, Marianne Tronstad Lund, and Dirk Olivié for giving us vertical distributions of

556 BC in the Arctic. [We thank Daven K. Henze, Forrest Lacey, and three anonymous reviewers for valuable](#)  
557 [comments that were helpful for the paper. We also thank the editor for his contributions.](#)

558 **References**

- 559 Aamaas, B., Peters, G., and Fuglestedt, J. S.: Simple emission metrics for climate impacts, *Earth Syst.*  
560 *Dynam.*, 4, 145-170, 10.5194/esd-4-145-2013, 2013.
- 561 Aamaas, B., Berntsen, T. K., Fuglestedt, J. S., Shine, K. P., and Bellouin, N.: Regional emission metrics  
562 for short-lived climate forcers from multiple models, *Atmos. Chem. Phys.*, 16, 7451-7468,  
563 10.5194/acp-16-7451-2016, 2016.
- 564 Bellouin, N., Baker, L., Hodnebrog, Ø., Olivie, D., Cherian, R., Macintosh, C., Samset, B., Esteve, A.,  
565 Aamaas, B., Quaas, J., and Myhre, G.: Regional and seasonal radiative forcing by perturbations to  
566 aerosol and ozone precursor emissions, *Atmospheric Chemistry and Physics*, 16, 13885-13910,  
567 10.5194/acp-16-13885-2016, 2016.
- 568 Bentsen, M., Bethke, I., Debernard, J. B., Iversen, T., Kirkevåg, A., Seland, Ø., Drange, H., Roelandt, C.,  
569 Seierstad, I. A., Hoose, C., and Kristjánsson, J. E.: The Norwegian Earth System Model, NorESM1-M –  
570 Part 1: Description and basic evaluation of the physical climate, *Geosci. Model Dev.*, 6, 687-720,  
571 10.5194/gmd-6-687-2013, 2013.
- 572 Boer, G. B., and Yu, B. Y.: Climate sensitivity and response, *Climate Dynamics*, 20, 415-429,  
573 10.1007/s00382-002-0283-3, 2003.
- 574 Boer, G. J.: The ratio of land to ocean temperature change under global warming, *Climate Dynamics*,  
575 37, 2253-2270, 10.1007/s00382-011-1112-3, 2011.
- 576 Boucher, O., and Reddy, M. S.: Climate trade-off between black carbon and carbon dioxide emissions,  
577 *Energy Policy*, 36, 193-200, 2008.
- 578 Bowman, K., and Henze, D. K.: Attribution of direct ozone radiative forcing to spatially resolved  
579 emissions, *Geophysical Research Letters*, 39, n/a-n/a, 10.1029/2012GL053274, 2012.
- 580 Cherubini, F., Fuglestedt, J., Gasser, T., Reisinger, A., Cavalett, O., Huijbregts, M. A. J., Johansson, D.  
581 J. A., Jørgensen, S. V., Raugei, M., Schivley, G., Strømman, A. H., Tanaka, K., and Lévassieur, A.:  
582 Bridging the gap between impact assessment methods and climate science, *Environmental Science &*  
583 *Policy*, 64, 129-140, <http://dx.doi.org/10.1016/j.envsci.2016.06.019>, 2016.
- 584 Collins, W. J., Fry, M. M., Yu, H., Fuglestedt, J. S., Shindell, D. T., and West, J. J.: Global and regional  
585 temperature-change potentials for near-term climate forcers, *Atmos. Chem. Phys.*, 13, 2471-2485,  
586 10.5194/acp-13-2471-2013, 2013.
- 587 Flanner, M. G.: Arctic climate sensitivity to local black carbon, *Journal of Geophysical Research:*  
588 *Atmospheres*, 118, 1840-1851, 10.1002/jgrd.50176, 2013.
- 589 Fry, M. M., Naik, V., West, J. J., Schwarzkopf, D., Fiore, A., Collins, W. J., Dentener, F., Shindell, D. T.,  
590 Atherton, C. S., Bergmann, D. J., Duncan, B. N., Hess, P. G., MacKenzie, I. A., Marmor, E., Schultz, M.  
591 G., Szopa, S., Wild, O., and Zeng, G.: The influence of ozone precursor emissions from four world  
592 regions on tropospheric composition and radiative climate forcing, *J. Geophys. Res.*, 117, D07306,  
593 10.1029/2011JD017134, 2012.
- 594 Fuglestedt, J. S., Berntsen, T. K., Godal, O., Sausen, R., Shine, K. P., and Skodvin, T.: Metrics of  
595 climate change: Assessing radiative forcing and emission indices, *Climatic Change*, 58, 267-331, 2003.
- 596 Fuglestedt, J. S., Shine, K. P., Berntsen, T., Cook, J., Lee, D. S., Stenke, A., Skeie, R. B., Velders, G. J.  
597 M., and Waitz, I. A.: Transport impacts on atmosphere and climate: Metrics, *Atmospheric*  
598 *Environment*, 44, 4648-4677, 2010.
- 599 Henze, D. K., Shindell, D. T., Akhtar, F., Spurr, R. J. D., Pinder, R. W., Loughlin, D., Kopacz, M., Singh,  
600 K., and Shim, C.: Spatially Refined Aerosol Direct Radiative Forcing Efficiencies, *Environmental Science*  
601 *& Technology*, 46, 9511-9518, 10.1021/es301993s, 2012.
- 602 Hewitt, H. T., Copesey, D., Culverwell, I. D., Harris, C. M., Hill, R. S. R., Keen, A. B., McLaren, A. J., and  
603 Hunke, E. C.: Design and implementation of the infrastructure of HadGEM3: the next-generation Met  
604 Office climate modelling system, *Geosci. Model Dev.*, 4, 223-253, 10.5194/gmd-4-223-2011, 2011.

605 IPCC: The Physical Science Basis. Contribution of Working Group I to the Fifth Assessment Report of  
606 the Intergovernmental Panel on Climate Change, edited by: Stocker, T. F., Qin, D., Plattner, G. K.,  
607 Tignor, M., Allen, S. K., Boschung, J., Nauels, A., Xia, Y., Bex, V., and Midgley, P. M., Cambridge  
608 University Press, Cambridge, United Kingdom and New York, NY, USA, 1535 pp., 2013.

609 Iversen, T., Bentsen, M., Bethke, I., Debernard, J. B., Kirkevåg, A., Seland, Ø., Drange, H., Kristjansson,  
610 J. E., Medhaug, I., Sand, M., and Seierstad, I. A.: The Norwegian Earth System Model, NorESM1-M –  
611 Part 2: Climate response and scenario projections, *Geosci. Model Dev.*, 6, 389-415, 10.5194/gmd-6-  
612 389-2013, 2013.

613 Joshi, M. M., Gregory, J. M., Webb, M. J., Sexton, D. M. H., and Johns, T. C.: Mechanisms for the  
614 land/sea warming contrast exhibited by simulations of climate change, *Climate Dynamics*, 30, 455-  
615 465, 10.1007/s00382-007-0306-1, 2008.

616 Klimont, Z., Höglund-Isaksson, L., Heyes, C., Rafaj, P., Schöpp, W., Cofala, J., Purohit, P., Borken-  
617 Kleefeld, J., Kupiainen, K., Kiesewetter, G., Winiwarter, W., Amann, M., Zhao, B., Wang, S. X., Bertok,  
618 I., and Sander, R.: Global scenarios of air pollutants and methane: 1990-2050, In prep.

619 Lund, M., Berntsen, T., Fuglestedt, J., Ponater, M., and Shine, K.: How much information is lost by  
620 using global-mean climate metrics? an example using the transport sector, *Climatic Change*, 113,  
621 949-963, 10.1007/s10584-011-0391-3, 2012.

622 Lund, M. T., Berntsen, T. K., Heyes, C., Klimont, Z., and Samset, B. H.: Global and regional climate  
623 impacts of black carbon and co-emitted species from the on-road diesel sector, *Atmospheric*  
624 *Environment*, 98, 50-58, <http://dx.doi.org/10.1016/j.atmosenv.2014.08.033>, 2014.

625 Myhre, G., Highwood, E., Shine, K. P., and Stordal, F.: New estimates of radiative forcing due to well  
626 mixed greenhouse gases, *Geophysical Research Letters*, 25, 2715-2718, 1998.

627 Myhre, G., Berglen, T. F., Johnsrud, M., Hoyle, C. R., Berntsen, T. K., Christopher, S. A., Fahey, D. W.,  
628 Isaksen, I. S. A., Jones, T. A., Kahn, R. A., Loeb, N., Quinn, P., Remer, L., Schwarz, J. P., and Yttri, K. E.:  
629 Modelled radiative forcing of the direct aerosol effect with multi-observation evaluation, *Atmos.*  
630 *Chem. Phys.*, 9, 1365-1392, 10.5194/acp-9-1365-2009, 2009.

631 Myhre, G., Shindell, D., Bréon, F.-M., Collins, B., Fuglestedt, J. S., Huang, J., Koch, D., Lamarque, J.-F.,  
632 Lee, D., Mendoza, B., Nakajima, T., Robock, A., Stephens, G., Takemura, T., and Zhang, H.:  
633 Anthropogenic and Natural Radiative Forcing, in: *Climate Change 2013: The Physical Science Basis.*  
634 *Contribution of Working Group I to the Fifth Assessment Report of the Intergovernmental Panel on*  
635 *Climate Change*, edited by: Stocker, T. F., Qin, D., Plattner, G. K., Tignor, M., Allen, S. K., Boschung, J.,  
636 Nauels, A., Xia, Y., Bex, V., and Midgley, P. M., Cambridge University Press, Cambridge, United  
637 Kingdom and New York, NY, USA, 2013.

638 Najafi, M. R., Zwiers, F. W., and Gillett, N. P.: Attribution of Arctic temperature change to  
639 greenhouse-gas and aerosol influences, *Nature Clim. Change*, 5, 246-249, 10.1038/nclimate2524,  
640 2015.

641 Olivié, D. J. L., and Peters, G.: Variation in emission metrics due to variation in CO<sub>2</sub> and temperature  
642 impulse response functions, *Earth System Dynamics*, 4, 267-286, 10.5194/esd-4-267-2013, 2013.

643 Quinn, P. K., Bates, T. S., Baum, E., Doubleday, N., Fiore, A. M., Flanner, M., Fridlind, A., Garrett, T. J.,  
644 Koch, D., Menon, S., Shindell, D., Stohl, A., and Warren, S. G.: Short-lived pollutants in the Arctic:  
645 their climate impact and possible mitigation strategies, *Atmos. Chem. Phys.*, 8, 1723-1735,  
646 10.5194/acp-8-1723-2008, 2008.

647 Samset, B. H., and Myhre, G.: Vertical dependence of black carbon, sulphate and biomass burning  
648 aerosol radiative forcing, *Geophysical Research Letters*, 38, L24802, 10.1029/2011GL049697, 2011.

649 Sand, M., Berntsen, T. K., Seland, Ø., and Kristjánsson, J. E.: Arctic surface temperature change to  
650 emissions of black carbon within Arctic or midlatitudes, *Journal of Geophysical Research:*  
651 *Atmospheres*, 118, 7788-7798, 10.1002/jgrd.50613, 2013.

652 Schmale, J., Shindell, D., von Schneidmesser, E., Chabay, I., and Lawrence, M.: Clean up our skies,  
653 *Nature*, 515, 335-337, 2014.

654 Shindell, D., and Faluvegi, G.: Climate response to regional radiative forcing during the twentieth  
655 century, *Nature Geoscience*, 2, 294-300, 2009.

656 Shindell, D., and Faluvegi, G.: The net climate impact of coal-fired power plant emissions, *Atmos.*  
657 *Chem. Phys.*, 10, 3247-3260, 10.5194/acp-10-3247-2010, 2010.

658 Shindell, D., Schulz, M., Ming, Y., Takemura, T., Faluvegi, G., and Ramaswamy, V.: Spatial scales of  
659 climate response to inhomogeneous radiative forcing, *Journal of Geophysical Research:*  
660 *Atmospheres*, 115, D19110, 10.1029/2010JD014108, 2010.

661 Shindell, D., Kuylenstierna, J. C. I., Vignati, E., van Dingenen, R., Amann, M., Klimont, Z., Anenberg, S.  
662 C., Muller, N., Janssens-Maenhout, G., Raes, F., Schwartz, J., Faluvegi, G., Pozzoli, L., Kupiainen, K.,  
663 Höglund-Isaksson, L., Emberson, L., Streets, D., Ramanathan, V., Hicks, K., Oanh, N. T. K., Milly, G.,  
664 Williams, M., Demkine, V., and Fowler, D.: Simultaneously Mitigating Near-Term Climate Change and  
665 Improving Human Health and Food Security, *Science*, 335, 183-189, 10.1126/science.1210026, 2012.

666 Shindell, D. T.: Evaluation of the absolute regional temperature potential, *Atmos. Chem. Phys.*, 12,  
667 7955-7960, 10.5194/acpd-12-7955-2012, 2012.

668 Shindell, D. T.: Inhomogeneous forcing and transient climate sensitivity, *Nature Clim. Change*, 4, 274-  
669 277, 10.1038/nclimate2136, 2014.

670 Shindell, D. T., Faluvegi, G., Rotstayn, L., and Milly, G.: Spatial patterns of radiative forcing and  
671 surface temperature response, *Journal of Geophysical Research: Atmospheres*, 120, 5385-5403,  
672 10.1002/2014JD022752, 2015.

673 Shine, K. P., Fuglestedt, J. S., Hailemariam, K., and Stuber, N.: Alternatives to the Global Warming  
674 Potential for Comparing Climate Impacts of Emissions of Greenhouse Gases, *Climatic Change*, 68,  
675 281-302, 10.1007/s10584-005-1146-9, 2005.

676 Stevens, B., Giorgetta, M., Esch, M., Mauritsen, T., Crueger, T., Rast, S., Salzmann, M., Schmidt, H.,  
677 Bader, J., Block, K., Brokopf, R., Fast, I., Kinne, S., Kornbluh, L., Lohmann, U., Pincus, R., Reichler, T.,  
678 and Roeckner, E.: Atmospheric component of the MPI-M Earth System Model: ECHAM6, *Journal of*  
679 *Advances in Modeling Earth Systems*, 5, 146-172, 10.1002/jame.20015, 2013.

680 Stohl, A., Aamaas, B., Amann, M., Baker, L. H., Bellouin, N., Berntsen, T. K., Boucher, O., Cherian, R.,  
681 Collins, W., Daskalakis, N., Dusinska, M., Eckhardt, S., Fuglestedt, J. S., Harju, M., Heyes, C.,  
682 Hodnebrog, O., Hao, J., Im, U., Kanakidou, M., Klimont, Z., Kupiainen, K., Law, K. S., Lund, M. T., Maas,  
683 R., MacIntosh, C. R., Myhre, G., Myriokefalitakis, S., Olivie, D., Quaas, J., Quennehen, B., Raut, J.-C.,  
684 Rumbold, S. T., Samset, B. H., Schulz, M., Seland, O., Shine, K. P., Skeie, R. B., Wang, S., Yttri, K. E., and  
685 Zhu, T.: Evaluating the climate and air quality impacts of short-lived pollutants, *Atmospheric*  
686 *Chemistry and Physics*, 15, 10529-10566, 10.5194/acp-15-10529-2015, 2015.

687 Søvde, O. A., Gauss, M., Smyshlyaev, S. P., and Isaksen, I. S. A.: Evaluation of the chemical transport  
688 model Oslo CTM2 with focus on arctic winter ozone depletion, *Journal of Geophysical Research:*  
689 *Atmospheres*, 113, D09304, 10.1029/2007JD009240, 2008.

690 Tol, R. S. J., Berntsen, T., O'Neill, B. C., Fuglestedt, J. S., and Shine, K.: A unifying framework for  
691 metrics for aggregating the climate effect of different emissions *Environmental Research Letters*, 7,  
692 044006, 10.1088/1748-9326/7/4/044006, 2012.

693

694

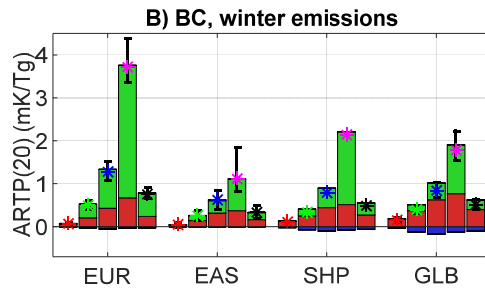
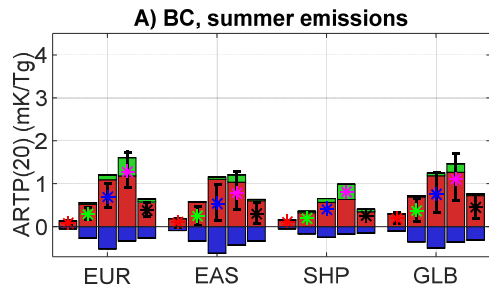
695 Table 1: The models and species included. Models are either general circulation models (GCM) or chemistry transport models  
 696 (CTM). The resolution column shows the horizontal resolution and the number of vertical layers.

Model	Type	Resolution	BC	OC	SO <sub>2</sub>	NH <sub>3</sub>	NO <sub>x</sub>	CO	VOC	CH <sub>4</sub>	References
ECHAM6-HAMMOZ	GCM	1.8°x1.8° L31	X	X	X						Stevens et al. (2013)
HadGEM3-GLOMAP	GCM	1.8°x1.2° L38	X	X	X		X	X	X	X	Hewitt et al. (2011)
NorESM	GCM	1.9°x2.5° L26	X	X	X		X	X	X	X	Bentsen et al. (2013); Iversen et al. (2013)
OsloCTM2	CTM	2.8°x2.8° L60	X	X	X	X	X	X	X	X	Søvde et al. (2008); Myhre et al. (2009)

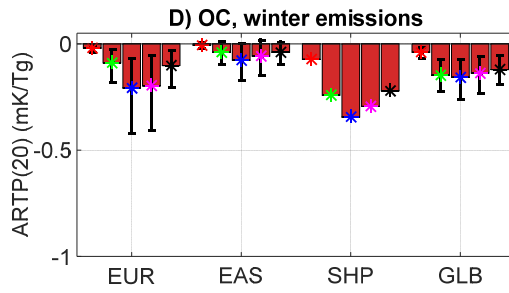
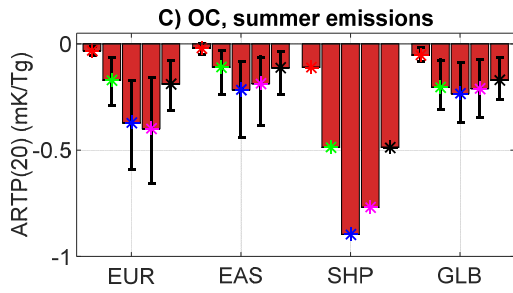
697

698

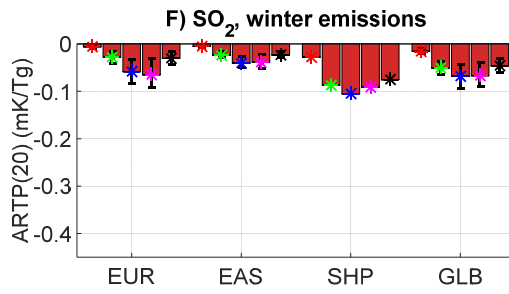
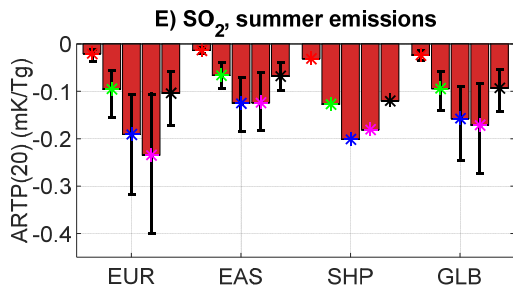
699



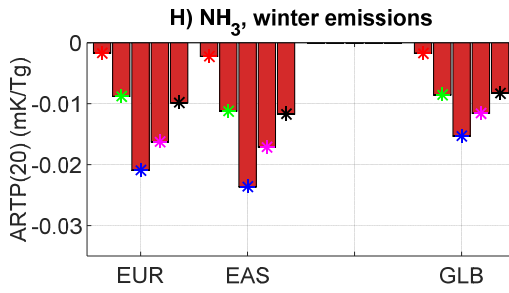
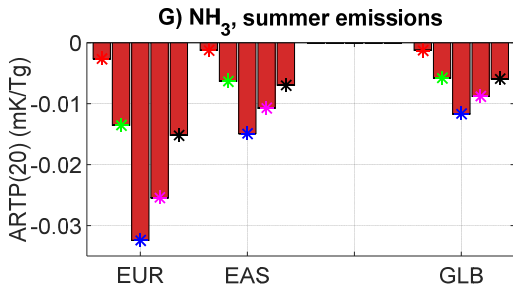
700



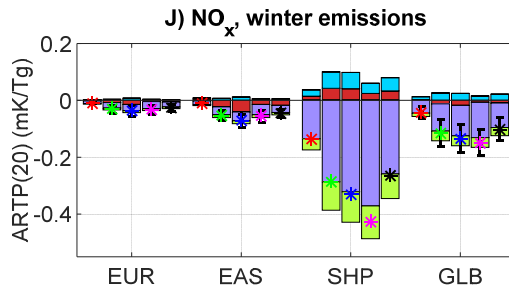
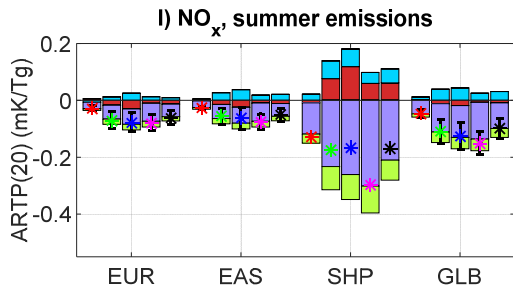
701



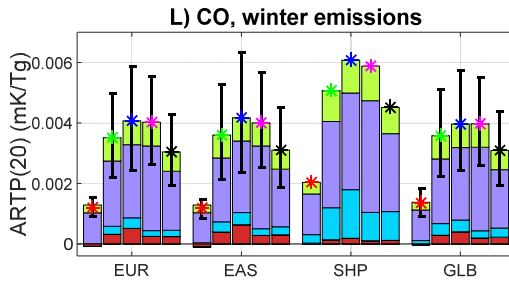
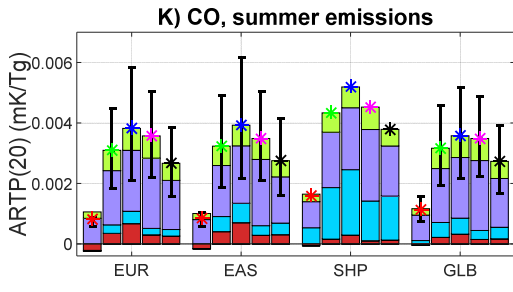
702



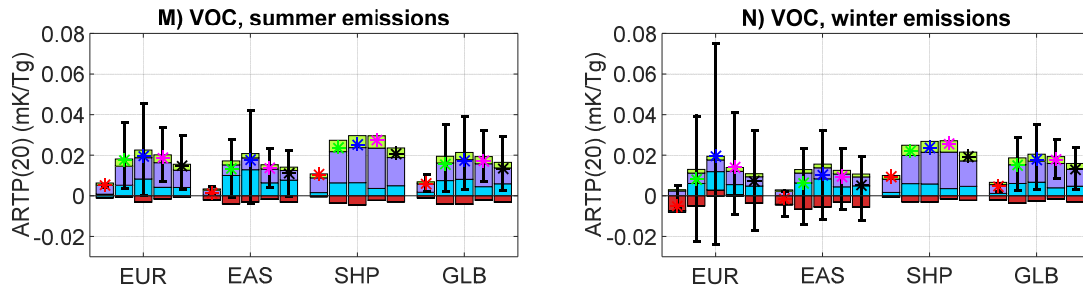
703



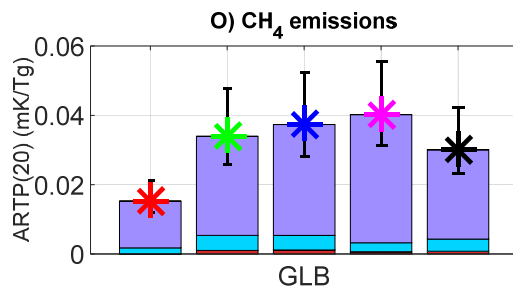
704



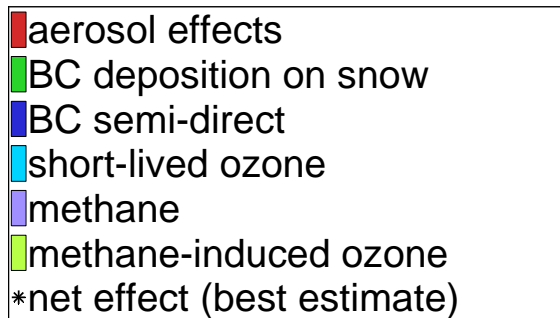
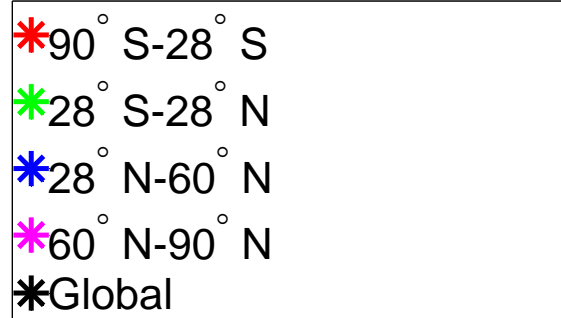




705

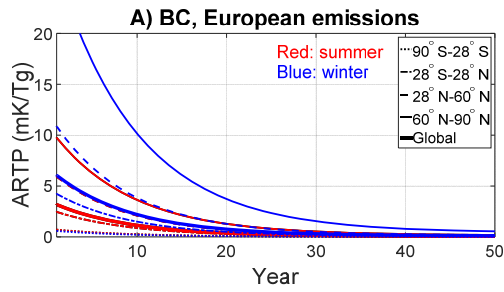


706

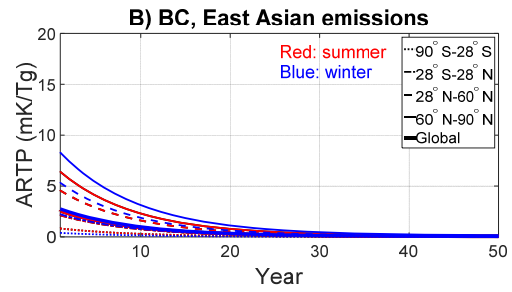


707

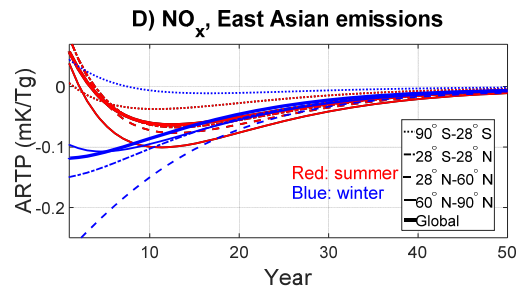
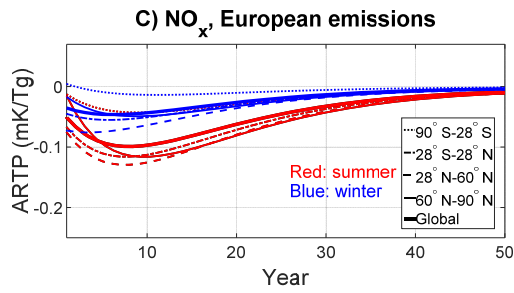
708 Figure 1: ARTP20 for emissions from Europe, East Asia, shipping, and global and for summer and winter. In each frame, and  
 709 for each emission region, the ARTP20 values for the four latitudinal response bands from south (left) to north (right), as well  
 710 as the global response average (rightmost), for the species, decomposed by *effects*~~processes~~. The net response is shown by the  
 711 asterisk. The regions included are Europe (EUR), East Asia (EAS), shipping (SHP), and global (GLB), all for both NH summer,  
 712 May-October (left), and NH winter, November-April (right). The uncertainty bars show the range across models, which is not  
 713 given for shipping as the best estimate is based on only two models for that sector. Due to the methodology applied, a fraction  
 714 of the semi-direct effect for BC in the Arctic is included in the *aerosol effects*~~process~~, as explained in Sect. 2.2.4. Note that the  
 715 vertical axis varies between different emitted components.



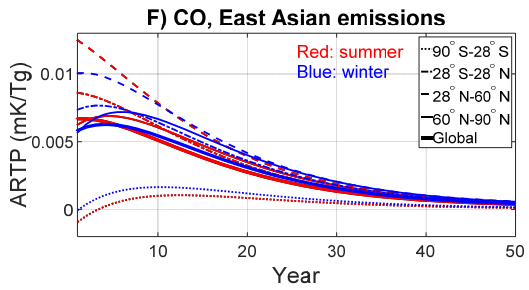
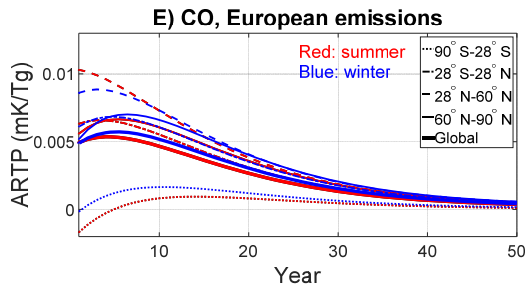
716



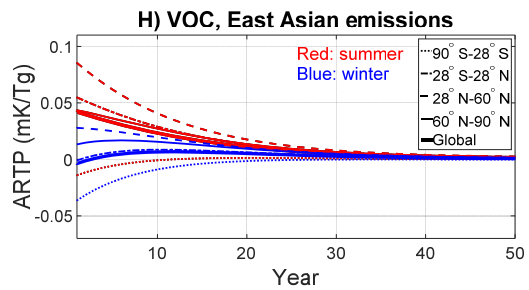
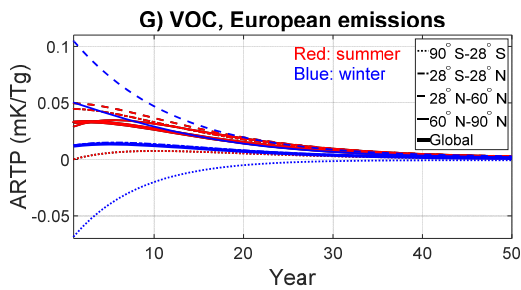
717



718



719



720

Figure 2: ARTP values in different response bands for BC and the ozone precursors for time horizons up to 50 years. Emissions

721

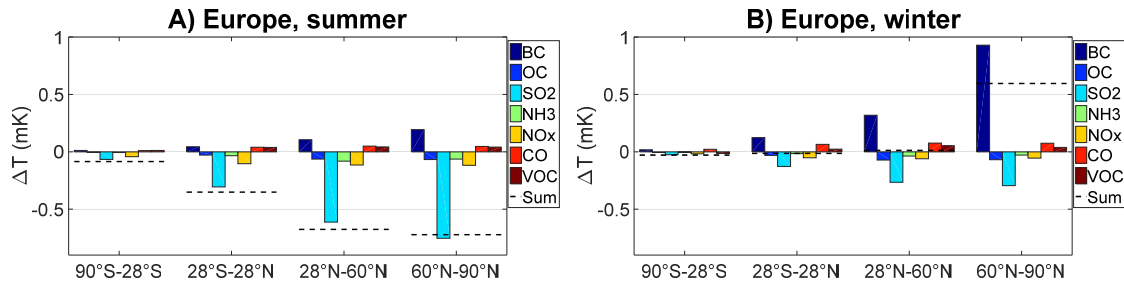
in Europe (left) and East Asia (right) in NH summer (May-October) are given as red and in NH winter (November-April) as

722

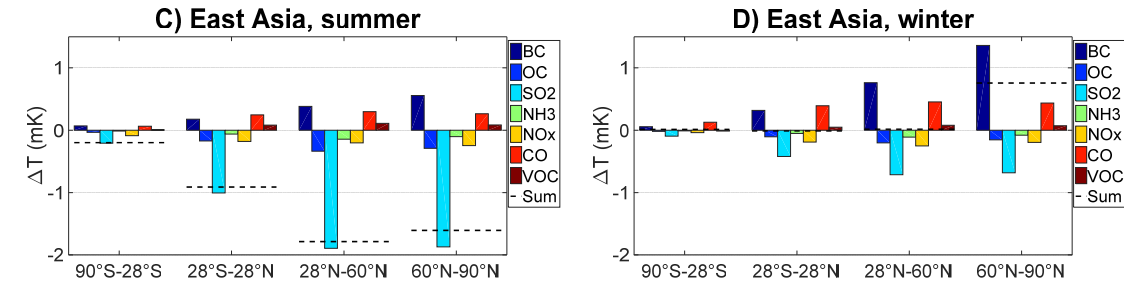
blue.

723

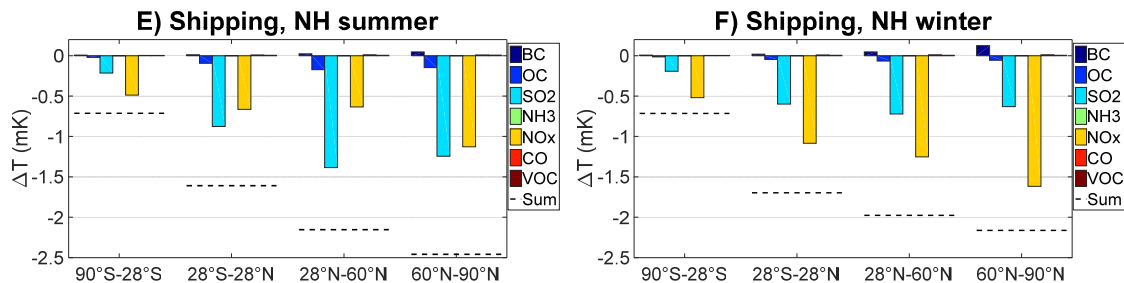
724



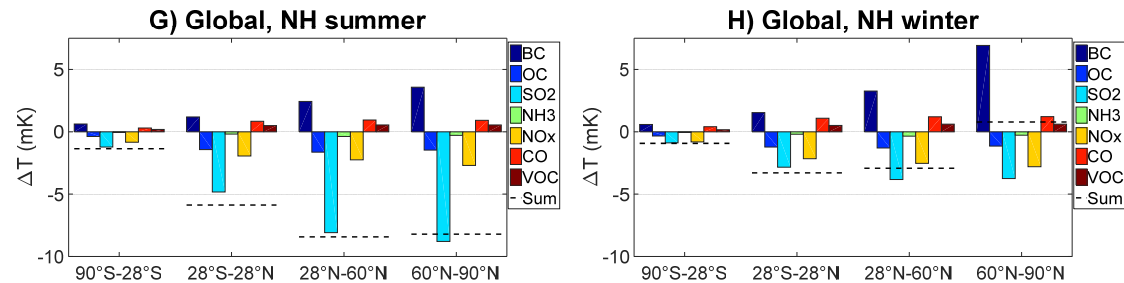
725



726

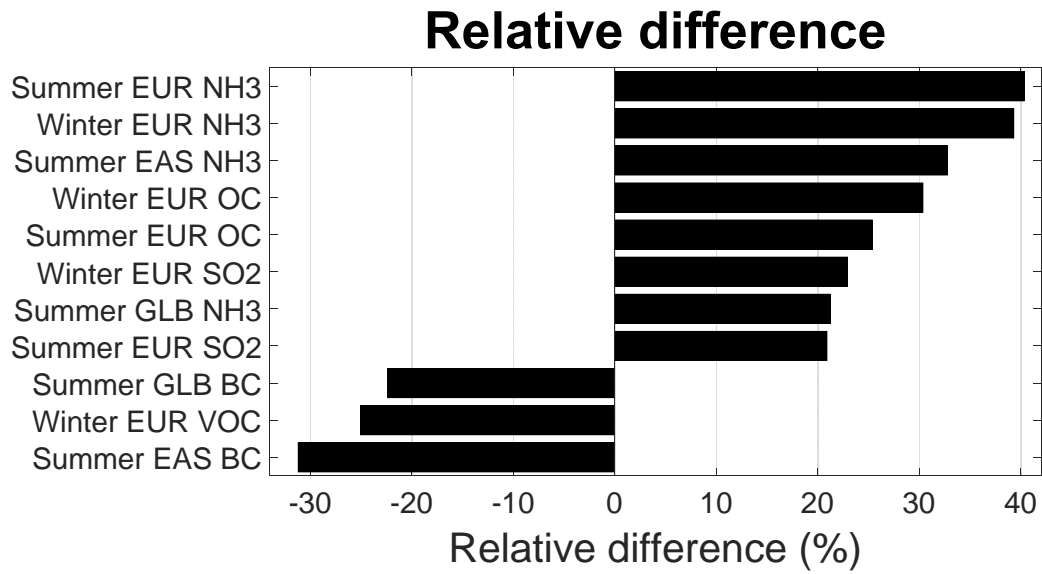


727



728 Figure 3: The regional temperature response for a time horizon of 20 years after regional and seasonal emissions in 2008 based  
 729 on ARTP(20). The four latitude response bands represent the SH mid-high latitudes, Tropics, NH mid-latitudes, and Arctic.  
 730 The global response average is given in Fig. S2. From top to bottom, the emission regions are Europe, East Asia, the global  
 731 shipping sector, and global. The emissions are split into NH summer season (May-October) to the left and NH winter season  
 732 (November-April) to the right. Note that the y-axis differs for the regions. The horizontal dashed lines show the sum for each  
 733 response band.

734



735

736 Figure 4: The relative difference between the global temperature responses based on ARTP and AGTP methods for a time  
 737 horizon of 20 years. Only cases with larger relative differences than 20% are shown. Positive numbers occur when the  
 738 magnitude of the global temperature response is larger when based on ARTP than on AGTP, negative when the magnitude is  
 739 largest based on AGTP.

740